Theoretical model of microlayer formation for isolated boiling bubble

Satbyoul Jung [a] and Hyungdae Kim [a*]
[a]Department of Nuclear Engineering, Kyung Hee University, Yongin, Republic of Korea

[*]Corresponding author: hdkims@khu.ac.kr

1. Introduction

When a vapor bubble grows on a heated surface, a thin liquid layer (microlayer) forms at the base. Evaporation of the microlayer plays an important role in bubble growth during nucleate boiling [1-3], with a strong dependence on the initial thickness of the microlayer δ_0. Thus, inaccurate prediction of the initial microlayer thickness leads to considerable error in the growth behavior of a single bubble, with accumulation generating physically unreasonable pictures for boiling heat transfer phenomena. Several classical models are available for prediction of initial microlayer thicknesses, including Cooper and Lloyd [1], Van Ouwerkerk [6], and Simirnov [7], however these significantly over-predict experimental microlayer thicknesses [3, 6]. Hence, recent advanced boiling simulations with a microlayer model have relied on a purely empirical correlation of the initial microlayer thickness [8, 9]. Despite the significance of the initial microlayer thickness and the inaccuracy of existing theoretical models, there has been no systematic study resolving the large discrepancy between the existing models and experimental data on initial microlayer thicknesses. The aim of this paper was to conduct a new experiment to aid the understanding of hydrodynamic phenomena during the formation of a microlayer underneath a boiling bubble, and to develop a sophisticated theoretical model for initial microlayer thickness that is in agreement with experiment.

2. Classical models

We review the classical theoretical models of initial microlayer thickness. Cooper and Lloyd [1] and Van Ouwerkerk [6] conducted theoretical modeling based on the assumption that the initial microlayer thickness is equal to the displacement thickness of the hydrodynamic boundary layer around a bubble, and obtained a simple prediction equation, $\delta_0 = C_0(vt)^{1/2}$, for a hemispherical bubble satisfying a growth law of $R = Ct^{0.5}$. The value of C_0 was chosen from an analysis of experimental data: 0.8 in [1] and 1.26 in [6]. Later, Smirnov [7] attempted to calculate the initial microlayer thickness by solving the continuity and linear momentum equations for the hydrodynamics of one-dimensional radial flow during formation of the microlayer. Using the assumption of a hemispherical bubble, the velocity at the microlayer boundary, $u_m(r,$

$\delta_0)$, was taken to be equal to that of the expanding bubble interface:

$$u_m(R,\delta_0) = \frac{dR_b}{dt} .\tag{1}$$

Then, the following equation is obtained:

$$\delta_0 = \sqrt{2vR \Big/ \left[-\frac{2}{\rho}\frac{dP}{dR} - \frac{d^2R}{dt^2} + \frac{2}{3}\left(\frac{dR}{dt}\right)^2 \frac{1}{R} \right]} .\tag{2}$$

The value of dP/dR can be determined using the Rayleigh-Plesset equation:

$$\frac{dP}{dR} = 4\frac{\partial^2 R}{\partial t^2} + \frac{R(d^3R/dt^3)}{dR/dt} - \frac{2\sigma}{\rho R^2 (dR/dt)} .\tag{3}$$

If the surface force for the rapid growth stage of the bubble is negligibly small and bubble growth follows the growth law in the form $R = Ct^n$, then Eq. (2) becomes:

$$\delta_0 = \sqrt{\frac{2vt}{9(1-n)+2\left(\frac{1}{n}-1\right)(n-2)+0.66n}} .\tag{4}$$

When the exponent of the bubble growth is chosen as n=0.5, Eq. (4) becomes $\delta_0 = C_0(vt)^{1/2}$, which is fairly consistent with others except for a slight difference in the constant.

3. Experiment

A new experiment to aid understanding of hydrodynamic phenomena during formation of the microlayer beneath a boiling bubble was conducted. Three optical measurement methods were used to precisely capture the microlayer profile as well as local hydrodynamic parameters of a growing bubble in a fully synchronized manner [Fig. 1(a)]. The boiling bubble shape was captured from the side using a high-speed video (HSV) camera [Fig. 1(b)]. The fringe patterns due to the microlayer beneath the boiling bubble were detected using laser interferometry [Fig. 1(c)] and were analyzed to calculate the microlayer thickness. However, the liquid-vapor interface geometry in the transition region between R_m and R_b in Figs. 1 (b) and (c) could not be detected using these methods as it is too thin to be visualized by the side-viewing camera and so bended that reflected laser light for interferometry cannot travel
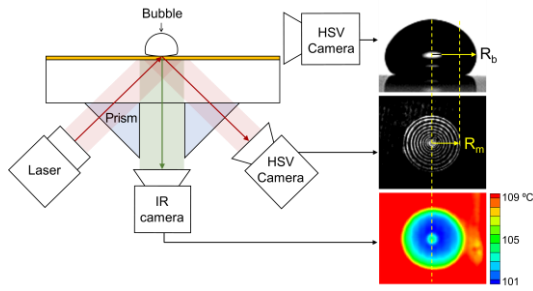
Fig. 1. (a) Schematic of experimental setup. (b)-(d) Images of a growing bubble, and corresponding fringe patterns and wall temperature distribution.

into the HSV camera. Instead, to detect the liquid-layer profile in the transition region, the wall temperature distribution was measured using a high-speed infrared (IR) camera [Fig. 1(d)]: the wall heat-flux distribution was calculated by solving the transient heat conduction in the heater plate using the measured temperature distribution as the boundary condition, then the liquid-layer thickness in the transition region and the microlayer were calculated using one-dimensional steady-state heat conduction through the microlayer, $q''_w = k_l(T_w-T_{sat})/\delta$ [10]. As a result, the complete geometry of a boiling bubble including the microlayer, the liquid-vapor interface in the transition region and the macroscopic bubble shape were experimentally determined using a combination of optical methods.

To facilitate use of the optical methods in combination, a 700 nm indium-tin-oxide (ITO) thin film heater on a 10 mm CaF_2 plate was used as a test specimen. Both the film heater and the base plate were transparent, to permit the use of visible light for laser interferometry. The base plate was transparent to infrared radiation, whereas the film heater was not, so a thermal image of the heater surface could be captured from below the base plate.

4. Results

We repeated the single bubble boiling experiment numerous times using saturated water under atmospheric pressure with a varying applied heat flux between 110-210 kW/m^2 and a corresponding wall superheat of 9-12°C. Figure 2 shows the evolution of the bubble geometry and microlayer profile taken from the measurement data for a representative experiment. The bubble growth data were fairly well matched with the well-known Mikic analytical solutions: $R{\sim}t$ and $R{\sim}t^{0.5}$ for the inertia- and thermal-controlled growth regimes, respectively [11] [Fig. 2(a)]. It was found that in the time period when microlayer formation mainly takes place at the bubble base (from 0.1 ms to 2.6 ms), bubble growth behavior is reasonably approximated with the functional form of the thermal-controlled growth regime, $R{\sim}t^{0.5}$. The proportional constant $t^{0.5}$ that best fits the experimental data was in the range 0.025-0.035 in this study.

The focus of this study was the isothermal hydrodynamic formation of the initial microlayer, neglecting its thinning due to liquid evaporation. However, the measured instantaneous microlayer profile does not arise only from isothermal hydrodynamic formation but also from thickness reduction due to evaporation. Thus, the true 'initial microlayer thickness profile' [solid symbol in Fig. 2(b)] was reconstructed from the instantaneous microlayer profiles [open symbols in Fig. 2(b)] by compensating for thickness reduction due to evaporation at each time step.

Now, we consider the geometry of the growing bubble during microlayer formation. The shape of a bubble growing on a flat surface is determined by competition between the inertial and surface tension forces [1, 11-13]: when a bubble grows quickly, the inertial force dominates and the resulting shape is hemispherical, whereas for slow bubble growth, the surface tension dominates and, thus, a spherical bubble forms. In our experiment, the bubble shape was oblate during the whole period of microlayer formation [Fig. 2(c)]. This indicates that both the inertia and surface tension forces had an effect on bubble growth. In addition, the oblate shape with a transition region results in a considerable difference between the radius of the bubble and the outer edge of the microlayer [Fig. 2(c)], with a ratio of approximately $R_b/R_m{\sim}0.6$. Therefore, the interface velocity sweeping liquid to form the microlayer was about half the bubble growth velocity.
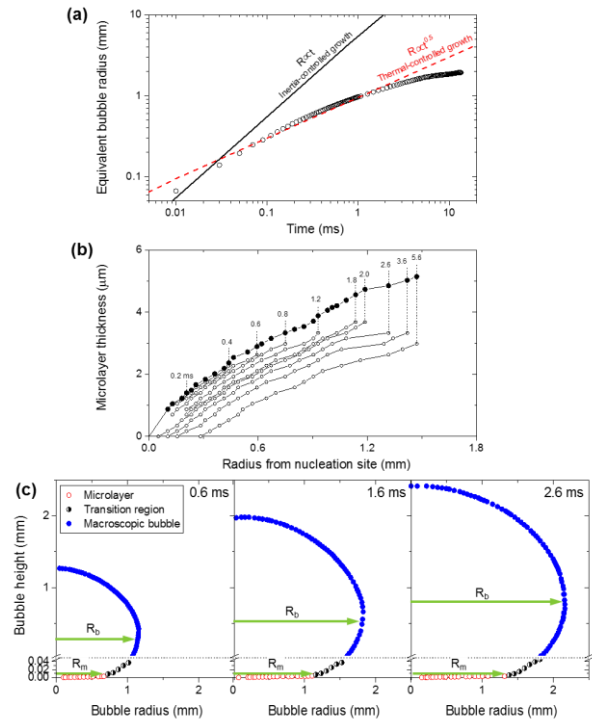
Fig. 2. (a) Equivalent bubble radius with time. (b) Time evolution of microlayer profile. The open and solid symbols represent the instantaneous thickness and the reconstructed thickness, respectively. (c) Bubble geometries including microlayer, transition region and macroscopic bubble.

5. Modelling

A significant discrepancy was observed between the experimental values of the initial microlayer thickness and results from classical models. Two clear distinctions can be identified as plausible reasons for this discrepancy. First, the surface tension term in Eq. (5) is neglected in the classical models while the oblate bubble shape in the experiment indicates that its effect is considerable. Second, in the classical models, the boiling bubble is approximated to be hemispherical and, thus, the microlayer formation velocity is the same as the bubble growth velocity, whereas in the experiment, an oblate bubble was observed and the interface velocity, sweeping liquid to form the microlayer, was considerably slower than the bubble growth velocity.

To reflect these two physical insights, the effects of surface tension and the difference in radius between the bubble and the microlayer were incorporated into the classical model derived by Smirnov [7]. First, the effect of surface tension on bubble growth can be taken into account by keeping the surface tension term when solving the Rayleigh-Plesset equation for the dynamics of a bubble, Eq. (3). For a growing bubble obeying $R_b = Ct^{0.5}$, the following microlayer thickness equation, including surface tension, is obtained:

$$\delta_0 = \sqrt{\frac{2vt}{9(1-n)+2\left(\frac{1}{n}-1\right)(n-2)+0.66n+\frac{4\sigma}{\rho C^4 n^2 t^{4n-3}}}} \; . \; (5)$$

In addition, the effect of the difference in radius between the bubble and the microlayer, $R_m/R_b = a$ ($a<1$), can be included by using $u_m = dR_m/dt = a(dR_b/dt)$ as the boundary condition at the outer edge of the microlayer in Eq. (1). For $a = 0.6$ from our experimental data, the following equation is obtained:

$$\delta_0 =$$

$$\sqrt{\frac{2vt}{\left(\frac{8}{a^3}+1\right)(1-n)+\frac{2}{a^3}\left(\frac{1}{n}-1\right)(n-2)+a^2 0.66n+\frac{4\sigma}{a^3 \rho C^4 n^2 t^{4n-3}}}}$$

$$(6)$$

These analyses incorporating the effects of surface tension and the bubble-microlayer radius difference result in sequential thinning of the microlayer, as seen in Fig. 3, because both lead to a decrease in sweep velocity and shear stress for microlayer formation. In addition, the initial microlayer thickness profile changes from linear to convex due to the increasing influence of surface tension in the denominator of Eqs. (7) and (8), which is consistent with the experimental observations. As a result of these two effects, the experimental data are more closely predicted by Eq. (8); however, a distinct discrepancy still remains.

There is one further physical aspect of microlayer formation that has not been considered so far, but that

may have a significant effect on the initial microlayer thickness. In the preceding analysis, residual flow in the microlayer was neglected because the characteristic timescale related to viscous friction in a thin liquid film, $t_r \sim \delta_0^2/v$, is very small (e.g., 10^{-3}-10^{-1} ms for a water liquid layer with thickness of 1-10 μm). As it is almost impossible to experimentally observe the short-lived residual flow, its influence has not been taken into account. However, there are some studies using numerical simulation that argue that the residual flow may have a considerable impact on the initial microlayer profile over such a short time interval [13, 14]. To give some indication of the importance of residual flow, we have attempted to estimate the residual flow effect on the initial microlayer thickness analytically. When stagnant liquid on a flat substrate is swept by a rapidly expanding bubble, the residual flow may further push the trapped liquid along the direction of bubble expansion and the microlayer thickness will be reduced by the amount of liquid pumped out by the residual flow. The equivalent amount of pumped liquid can be estimated by integrating the volumetric flow rate of the residual flow during its characteristic time and, thereby, the reduced thickness can be predicted. If we approximate the microlayer as an axisymmetric wedge, the resultant thickness (δ_r) incorporating the effect of residual flow can be given by:

$$\delta_r = \left(1 - \frac{3}{2}\frac{\overline{u_r}}{u_m} + \frac{1}{2}\left(\frac{\overline{u_r}}{u_m}\right)^3\right)\delta_0 \; , \qquad (7)$$

where δ_0 is the initial microlayer thickness without residual flow, u_m is the microlayer formation velocity and $\overline{u}_r$ is the average velocity of the residual flow. The velocity evolution of the residual flow can be simply presumed to follow the viscous diffusion equation, $\rho(\partial u_r/\partial t) \sim \mu(\partial^2 u_r/\partial y^2)$, which gives an approximate solution $u_r(t) = u_m \cdot \exp(-\mu t/\rho\delta^2)$. The effective residual flow dissipation time, t_r, for movement 95% of the terminal moving distance of the velocity solution ($l_r=0.95l_\infty$), $\overline{u}_r/u_m$ is about 0.32.

The proposed model shows remarkable agreement with the experimental data measured in the present study (Fig. 3). The model was further validated by comparing experimental data from other studies [1, 5, 15], which present quantitative data for bubble growth history as well as microlayer thickness. It was found that when the constant C in the equation $R = Ct^{0.5}$ is determined to best fit the bubble growth presented in each study, the proposed model predicts experimental results well, regardless of the liquid (water, toluene or methanol) or pressure conditions [Fig. 4]. Therefore, we can conclude that the proposed model appropriately reflects the major hydrodynamic mechanisms of initial microlayer formation underneath a growing bubble on a heated wall.
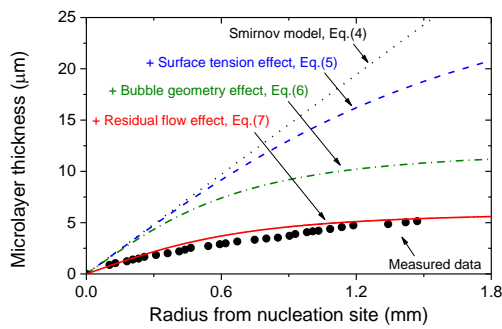
Fig. 3. Comparison of experimental data with the proposed model.
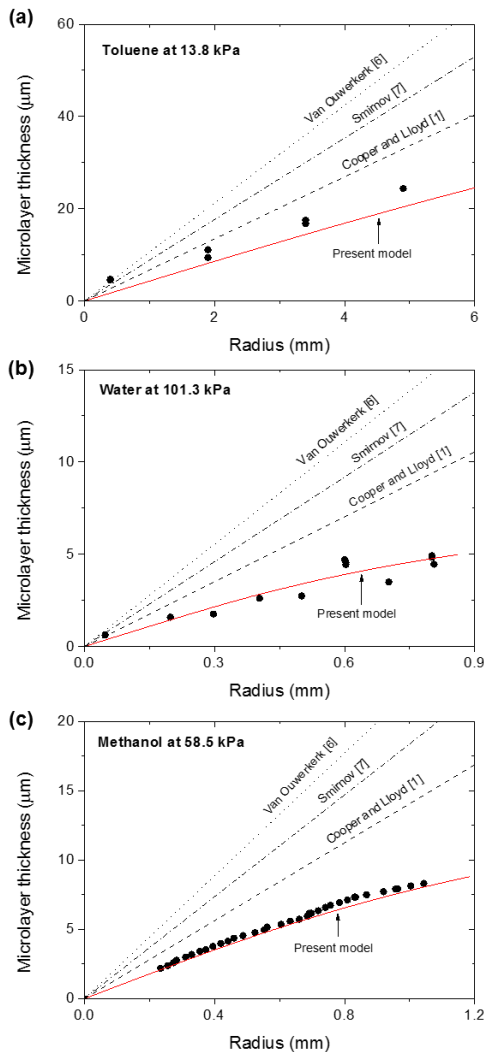
Fig. 4. Comparison of experimental data for initial microlayer thickness with theoretical models: (a) saturated toluene at 13.8 kPa [1], (b) saturated water at 101.3 kPa [5] and (c) saturated methanol at 58.5 kPa [15].

5. Conclusion

In conclusion, we studied the hydrodynamic formation of the microlayer beneath a vapor bubble growing on a heated surface in a stagnant pool. Classical models contain several idealizations (hemi-spherical bubble shape and neglecting surface tension effects), and significantly overestimate the initial microlayer thickness relative to experimental results. Precise observation of the growing bubble geometry during microlayer formation indicates that the bubble is oblate with a transition region between the microlayer and the macroscopic liquid, which reveals that surface tension plays a role in the process. This study also demonstrates the critical role played by the short-lived residual flow in microlayer formation. A theoretical model that incorporates the effects of surface tension, bubble geometry and residual flow has been shown to be in good general agreement with experimental data for various fluids from this and other studies.

REFERENCES

[1] M. G. Cooper and A. J. P. Lloyd, The microlayer in nucleate pool boiling, Int. J. Heat Mass Transfer, Vol. 12, p. 895, 1969.
[2] R. L. Judd and K. S. Hwang, A comprehensive model for nucleate pool boiling heat transfer including microlayer evaporation, ASME J. Heat Transfer, Vol. 98, p. 623, 1976.
[3] L. D. Koffman and M. S. Plesset, Experimental observations of the microlayer in vapor bubble growth on a heated solid, Journal of Heat Transfer, Vol. 105, p. 625, 1983.
[4] S. Jung and H. Kim, An experimental method to simultaneously measure the dynamics and heat transfer associated with a single bubble during nucleate boiling on a horizontal surface, Int. J. Heat Mass Transfer, Vol. 73, p. 365, 2014.
[5] T. Yabuki and O. Nakabeppu, Heat transfer mechanisms in isolated bubble boiling of water observed with MEMS sensor, Int. J. Heat Mass Transfer, Vol. 76, p. 28, 2014.
[6] H. J. Van Ouwerkerk, The role of the evaporating microlayer and dry surface areas in boiling (Ph. D. dissertation), Eindhoven University of Technology, 1970.
[7] G. F. Smirnov, Calculation of the initial thickness of the microlayer during bubble boiling, J. Engineering Physics, Vol. 28, p. 503, 1975.
[8] Y. Sato and B. Niceno, A depletable micro-layer model for nucleate pool boiling, J. Computational Physics, Vol. 300, p. 20, 2015.
[9] Y. Sato and B. Niceno, Nucleate pool boiling simulations using the interface tracking method: Boiling regime from discrete bubble to vapor mushroom region, Int. J Heat Mass Transfer, Vol. 105, p. 505, 2017.
[10] S. Jung and H. Kim, An experimental study on heat transfer mechanisms in the microlayer using integrated total reflection, laser interferometry and infrared thermometry technique, Heat Transfer Engineering, Vol. 36, p. 1002, 2015.
[11] B. B. Mikic, W. M. Rohsenow and P. Griffith, On bubble growth rates, Int. J. Heat Mass Transfer, Vol. 13, p. 657, 1970.
[12] M. A. Johnson, Jr. Javier De La Pena and R. B. Mesler, Bubble shape in nucleate boiling, AIChE Journal, Vol. 12, pp. 344, 1966.
[13] S. Hansch and S. Walker, The hydrodynamics of microlayer formation beneath vapour bubbles, Int. J. Heat Mass Transfer, Vol. 102, p. 1282, 2016.
[14] H. S. Fath, Microlayer formation, evaporation and bubble growth in nucleate boiling (Ph. D. dissertation), McMaster University, 1981.
[15] H. G. MacGregor and H. H. Jawurek, High speed cine laser interferometry technique for microlayer studies in boiling, N&O Joernaal, Vol. 4, p. 1, 1992.